The Influence of Multiple Slip Systems on the Brittle-Ductile Transition in Silicon

Brook D. Ferney and K. Jimmy Hsia*

Department of Theoretical and Applied Mechanics
University of Illinois at Urbana-Champaign
Urbana, IL 61801, USA

Submitted to: *Material Science and Engineering A*

February, 1999

* Corresponding author. Fax: (217)244-5707, e-mail: kj-hsia@uiuc.edu

Abstract

The brittle–ductile transition results from the competition between cleavage fracture and dislocation activities at or near the crack tip. In the present paper, a 2D dynamic dislocation simulation is performed. The material properties used in the simulation are those of single crystalline silicon. Dislocations are assumed to emit from an atomically sharp cleavage crack along different, symmetrically placed slip systems. Individual dislocations move away from the crack tip following an Arrhenius law driven by the net resolved shear stress. The dislocations shield the crack tip from the increasing far field stress intensity. Brittle fracture occurs when the crack tip stress intensity reaches the intrinsic fracture toughness. Ductile failure is assumed to occur if the far field stress intensity reaches a critical value significantly higher than the intrinsic toughness. The study focuses on the influence of interaction forces between dislocations in different slip systems. With all interactions fully accounted for, the simulations show that the activation of multiple slip systems results in a sharp transition whereas the activation of a single symmetric pair results in a gradual transition.

Keywords: Brittle-ductile transition; Fracture; Dislocation dynamics; Numerical simulation; Silicon

1. Introduction

The brittle-ductile transition (BDT) during fracture of engineering materials has been a subject of extensive research because of its practical significance. Transition from ductile fracture under ambient conditions to brittle fracture at low temperatures or high strain rates is a limiting constraint in the use of many structural metals. With the recently renewed interest in the *Titanic*, the subject appears even in publications for the layman [1]. It is now understood that the mechanism controlling the BDT during fracture in crystalline materials is the competition between two crack tip processes: cleavage crack propagation and dislocation activities at the crack tip. Although the cleavage fracture process is relatively well understood, the dislocation generation process is still actively studied by many researchers.

Of all engineering materials, steels are perhaps the most important ones exhibiting the BDT behavior. However, in order to understand the fundamental mechanisms of the brittle-ductile transition, single crystalline silicon has been extensively studied as a model material both experimentally [2-4] and numerically [5-12]. The dislocation generation process in silicon consists of dislocation nucleation at or near the crack tip (intrinsic silicon crystals are nearly dislocation-free) and dislocation motion away from the crack tip. Dislocation emission from a crack was first modeled by Rice and Thomson [13]. However, their calculations showed that the activation energy for dislocation emission for brittle materials as well as for transition metals was much too high to allow the BDT even when the temperature approaches the melting temperature. More recently, Rice and co-workers [14, 15] developed a model based on analysis of nonlinear atomic lattice distortion and identified an unstable stacking energy as the critical parameter for dislocation emission from a perfect crack tip. Their model still predicted a rather high barrier for dislocation emission. Recently, Xu *et al.* [16] studied dislocation nucleation from crack front defects theoretically and showed that the preferred dislocation nucleation sites are atomic ledges along the crack front. On the other hand, Kantha *et al.* [17] proposed a homogeneous dislocation loop formation mechanism due to thermal fluctuation. There is experimental evidence that dislocation nucleation in silicon can occur at temperatures significantly below the BDT temperature [3, 18, 19]. Therefore, the BDT in silicon is controlled by dislocation mobility rather than by dislocation nucleation.

Experiments also showed that the BDT in silicon is extremely sharp. Slightly below the transition temperature, the measured fracture toughness is nearly the intrinsic toughness of the material. At this temperature there is a tremendous increase in the measured fracture toughness accompanied by an increase in dislocation activity. Above this temperature, the material undergoes large scale yielding. For silicon with no built-in dislocations, the transition often occurs within as little as 5°C. This phenomenon of a very sharp transition seems to be at odds with the dislocation mobility controlled transition mechanism since dislocation mobility increases gradually with temperature. The purpose of the present paper is to identify a possible mechanism that may give rise to a relatively sharp transition during mobility controlled BDT.

It has often been argued that, in order to have a sharp transition, a large number of dislocations must be generated abruptly at the transition temperature [17]. There are, however, other possible mechanisms responsible for a sharp transition. Recently, Michot [20] showed that cross slip of dislocations near the crack tip is a plausible mechanism for

dislocation multiplication. Activation of multiple slip systems is another mechanism that has not been thoroughly studied.

Many numerical models have been developed to determine and understand the mechanisms causing the BDT behavior in silicon. The more successful ones among these were developed by the Oxford group [5-8]. Based on the argument that dislocation nucleation from the crack tip is inhomogeneous (a fact observed in many experiments [18, 21-23]), they introduced in their model the spacing between dislocation sources along the crack front. Their numerical simulations using this model result in a rather sharp transition and agree with experimental measurements. However, the value of the spacing between dislocation sources used in their simulation seems to be rather large compared with experimental results [18, 21]. Furthermore, many experiments show that multiple slip systems are activated at the crack tip during the BDT. The effect of multiple slip systems was not considered in their models.

Li and coworkers [24-27] studied the equilibrium arrangements of dislocations on single and multiple planes around the crack tip in order to understand the plastic zone and dislocation-free zone. These static models are not useful for studying the BDT since equilibrium is reached on a time scale much greater than that of a fracture test [6]. The resulting differences will be explained later in the discussion section. Of all dislocation dynamics simulations, only Brede [9] and Xin and Hsia [10] considered the influence of multiple slip systems. Brede [9] obtained a sharp transition by forcing simultaneous emission of dislocations on slip planes at 67.8° and –112.2° from the crack plane. He noted that including more slip systems might be necessary for modeling a sharp transition. Xin and Hsia [10] modeled dislocation emission in a pair of slip systems normal to the crack plane. The interactions between dislocations in different planes were not taken into account. They approximated the effect of multiple slip systems by multiplying the shielding term for a single slip system by a constant coefficient. This approximation showed the qualitative trend that an increase in the number of activated slip systems sharpens the transition behavior. The present study extends their simulation by accounting for the interactions between different slip systems. In particular, the effect of the number of active slip systems will be studied.

2. Simulation algorithm

Two-dimensional numerical simulations similar to those by Xin and Hsia [10] are performed. We consider {110} crack surfaces with a <110> crack growth direction. Silicon has a diamond-cubic structure with {111} slip planes and <110> slip directions. An analysis of the resolved shear stress for various slip systems shows that slip occurs initially in only four of the twelve available slip systems [10]. Such slip will not generate a perfectly two-dimensional deformation around the crack tip. Furthermore, once dislocations are nucleated from the crack front, the crack will no longer be perfectly planar. The crack front will contain many atomic steps at the locations where dislocation lines intercept the crack. However, for the problem to be tractable, we consider an atomically sharp crack from which straight edge dislocations are nucleated parallel to the crack front. Based upon X-ray topographs for this orientation by George and Michot [21], it was assumed that slip would occur symmetrically about the crack plane.

This model with a single pair of slip systems at a general angle α is illustrated in Fig. 1. Since the shear stresses are symmetric, the nucleation and subsequent motion of

dislocations in symmetric slip systems are also symmetric. When multiple slip systems are included in the model the different pairs of slip systems act independently. At each time step nucleation was tested on every pair of slip systems and occurred only in the pair, if any, which satisfied the stress condition explained later. The external load and slip system symmetry assure a pure mode I loading of the crack.

The total shear stress acting upon a given dislocation can be decomposed into three components. These may be expressed for the *i*th dislocation as [28]

$$\tau_i = \tau_{\mathrm{kd}} + \tau_{\mathrm{d}^2} + \sum_j \tau_{\mathrm{dd}_j} \tag{1}$$

where τ_{kd} is due to the crack tip stress field, τ_{d^2} is the image stress due to the crack faces, and τ_{dd_j} is the interaction stress due to the *j*th dislocation in the presence of the crack. To avoid a removable singularity found in [28], these terms can be expressed in terms of complex variables using the results of Lakshmanan and Li [24] as

$$\tau_{\mathrm{kd}} = \frac{K_I^{\infty}}{\sqrt{2\pi|z_i|}} \sin\left(\frac{\theta_i}{2}\right) \cos^2\left(\frac{\theta_i}{2}\right)$$

$$\tau_{\mathrm{d}^2} = \frac{\mu}{2\pi(1-\nu)} \left[\cos(2\phi_i)\mathrm{Re}(B_x + B) - \sin(2\phi_i)\mathrm{Im}(B_x + B)\right] \tag{2}$$

$$\tau_{\mathrm{dd}_j} = \frac{\mu}{2\pi(1-\nu)} \left[\cos(2\phi_i)\mathrm{Re}(B_x + B_{0x} + B + B_0) - \sin(2\phi_i)\mathrm{Im}(B_x + B_{0x} + B + B_0)\right]$$

where K_I^{∞} is the far-field stress intensity, z_i is the position of the *i*th dislocation measured in the complex plane with origin at the crack tip, θ_i and ϕ_i are the slip plane angle and Burgers vector angle, respectively, for the *i*th dislocation as shown in Fig. 1, μ is the shear modulus, ν is the Poisson's ratio, B_x, B, B_0, and B_{0x} are functions of complex variables derived in [24] and given explicitly in the Appendix, and Re(.) and Im(.) represent the real and imaginary parts of the complex function in the brackets.

A dislocation moves away from the crack tip if the shear stress acting upon it is greater than the lattice friction stress, τ_f, i.e. $\tau_i > \tau_f$. Its motion is a thermally activated glide process with the velocity obeying an Arrhenius-type relation, given by

$$v_i = v_0 \left(\frac{\tau_i - \tau_f}{\tau_0}\right)^m \exp\left(-\frac{Q}{kT}\right) \tag{3}$$

where v_0 and τ_0 are the material specific reference dislocation velocity and reference shear stress, respectively, m is the stress exponent, Q is the activation energy for dislocation glide, k is the Boltzmann constant, and T is the absolute temperature. The material properties used in this simulation are given in Table 1. The material constants in equation (3) are determined from Imai and Sumino [29] with τ_f chosen to fit their data for *p*-type, heavily doped silicon.

Table 1 Material properties for Si used in this simulation

μ	ν	K_{Ic}	B	r_0	τ_f	v_0	τ_0	Q	m
60.5	0.215	0.95	0.384	4	5	1.0×10^4	1	2.2	1
GPa		$\mathrm{MPa}\sqrt{\mathrm{m}}$	nm	nm	MPa	m/s	MPa	eV	

The simulation procedure is as follows. With a given loading rate, $\dot{K}_I^\infty$, and a specified temperature, T, the simulation proceeds by marching forward by constant time steps Δt. For each time step, the far-field stress intensity, K_I^∞, and the shear stress on each dislocation are calculated. If the stress on the ith dislocation is greater than the lattice friction stress, then the dislocation moves a distance $v_i \Delta t$. The magnitude of the time step is chosen such that during the entire simulation no dislocation will move beyond the position of the next farthest dislocation at the previous time.

Dislocations are assumed to nucleate at a distance r_0 from the crack tip in a designated slip system when the dislocation nucleation condition is satisfied. The distance r_0 is approximately the dislocation core width [9] and is given in Table 1. For each time step, a new dislocation is placed at r_0 and the resolved shear stress acting on this dislocation is calculated. If the shear stress is sufficient for the new dislocation to move then the dislocation remains. Otherwise it is removed. For the parameters used in this simulation, at least one dislocation was nucleated on every slip plane. Thus $K_I^\infty / K_{Ic} > 1$ even for brittle fracture.

The simulation continues until either cleavage fracture or ductile failure occurs. Cleavage fracture occurs when the local crack tip stress intensity, K_I^{tip}, reaches the intrinsic fracture toughness, K_{Ic}, where K_I^{tip} is calculated as [24]

$$K_I^{tip} = K_I^\infty - \sum_i \frac{b\mu}{(1-\nu)\sqrt{2\pi|z_i|}} \left\{ \frac{1}{2}\sin\left(\phi_i + \frac{\theta_i}{2}\right) - \frac{3}{4}\sin\left(\frac{\theta_i}{2} - \phi_i\right) + \frac{1}{4}\sin\left(\frac{5\theta_i}{2} - \phi_i\right) \right\} \quad (4)$$

where b is the magnitude of the Burgers vector. Ductile failure occurs when the crack tip shielding by the emitted dislocations is sufficient to prevent the crack tip from reaching the Griffith condition. It is assumed to occur when the applied stress intensity is sufficiently larger than the intrinsic fracture toughness. In the present simulation, ductile failure is assumed to occur when $K_I^\infty \geq 7\ K_{Ic}$. Seven was chosen based upon experimental results [3]. However, its actual magnitude does not affect the BDT temperature significantly for sharp transitions.

3. Effect of including interactions between different slip systems

From dislocation theory, it is known that the interaction force between two dislocations of the same sign lying in roughly the same plane is repulsive. From this perspective, it may be argued that including the interaction stresses from dislocations on the other side of the crack should aid dislocation motion. This increased mobility may lower the brittle-ductile transition temperature and increase the sharpness of the transition. However, this is not the case due to the nature of the crack-dislocations system.

The τ_{dd_j} term in equation (1) represents the interaction shear stress between two dislocations in the presence of the crack. This interaction stress is illustrated in Fig. 2, in which the stress acting upon a dislocation at $z_i=(r_i,\theta_i)$ by a dislocation at the variable position $z_j=(r_j,\pm\theta_i)$ is plotted versus r_j. Negative r_j corresponds to the $-\theta_i$ branch of the symmetric pair. The Burgers vector for each branch is shown in Fig. 1. In Fig. 2, the crack lies along the negative τ-axis with the crack tip at the origin. Positive interaction stress indicates that the dislocation at r_i is pushed away from the crack tip, whereas negative stress drives the dislocation toward the crack tip. The interaction stresses are

shown for three paired systems in silicon with angles of 45°, 90° and 135°. Figure 2 shows that when the two dislocations are in the same branch (i.e., when $r_j > 0$) the interaction stress drives the dislocation at r_i away from the crack when $r_j < r_i$ and drives it toward the crack when $r_j > r_i$. However, an interesting result was obtained when the two dislocations are in different branches (i.e., when $r_j < 0$). For the 45° and 90° pairs, the stress is positive if $|r_j| < r_i$ and negative when $|r_j| > r_i$; whereas the sign of the stress is reversed for the 135° pair. The interaction between the dislocations can therefore be repulsive or attractive depending upon relative location and slip plane angle. The crossover between the two behaviors occurs between 104° and 105°. For all angles, the magnitude of the interaction stress caused by dislocations in the opposite branch is much smaller than that caused by dislocations in the same branch. Angles of interest for silicon would lie between 45° and 135° where shielding can be significant. Plots of interaction stresses for smaller angles reveal more oscillatory behavior in the negative branch that is not explored here. It is significant that the stress vanishes at the symmetric position, i.e. $r_j=-r_I$, as noted by Lakshmanan and Li [24]. They also found that the net effect of interactions between symmetric slip systems could be repulsive or attractive depending upon the angle, but not at the same angles that we found.

There have been some concerns about the stability of symmetric models [11]. It was argued that initially symmetrically placed dislocation pairs may deviate from the symmetric arrangement as they move under applied stress, even under pure Mode I crack tip stress intensity. Such concern was investigated in this study. As noted above the interaction stress between two symmetrically placed dislocations is zero so they do not simply drive each other away from the crack tip. In a simulation of a pair of symmetric slip systems with a single dislocation in each slip plane under constant applied stress intensity, we found that the dislocations move outward to equilibrium positions influenced mainly by the *K*-field. There is a small influence of the image stresses and a very small influence of the interaction term. Because the *K*-field is so dominant, the dislocations tend to end up in symmetric equilibrium positions even when they started asymmetrically. The process of approaching symmetric positions is slightly retarded for 45° and 90° systems by the interaction stress, which tends to drive the dislocations away from symmetry. Likewise, it is enhanced for the 135° system since the interaction stress tends to drive the dislocations toward symmetry (see Fig. 2).

Although the magnitude of interaction stresses between different slip systems is small compared with that of other stress components, their effect on the transition behavior is significant. Such effect is illustrated in Figs. 3 and 4, which show the applied stress intensity and total number of emitted dislocations at fracture as functions of temperature. Each of the three angular pairs is simulated separately both with and without inter-branch interactions. Figures 3 and 4 show that including the interactions for the 45° and 90° pairs causes the brittle-ductile transition to shift to a higher temperature and to become more gradual. Including the interactions for the 135° pair provides some shielding where there was effectively none when inter-branch interactions were not accounted for. All of these two slip system models with the inter-branch interactions accounted for predict a gradual transition, which is not in agreement with experimental observations for silicon where the transition is very sharp. In the following section, the effect of multiple slip planes is considered to investigate how the number of active slip systems affects the sharpness of the transition.

4. Simulation with multiple slip systems

Using X-ray topography, George and Michot [21] observed that multiple slip systems were activated around crack tips in silicon near the transition temperature. For the crack tip orientation considered in the present study (i.e., {110} crack plane and <110> crack growth direction), they found that, of the twelve possible slip systems, five were always activated, three were activated in some cases, and four were never activated. The challenge of using a two-dimensional model is that some approximation must be made in choosing the slip plane angles. We chose angles of ±45° and ±135° since these are the angles of the Burgers vectors projected onto the *x*-*y* plane for this crystallographic orientation. A pair of ± 90° planes was also chosen to be consistent with [10], to give a good spacing with the other planes, and to be in the direction of some of the slip traces emerging at the specimen surface. These planes seem reasonable after viewing the X-ray topographs for this orientation by George and Michot (see gamma configuration in Fig. 6 of [21]).

To illustrate the effects of multiple slip systems two further cases were explored: one with four slip systems (±45° and ±135°) and one with six slip systems (±45°, ±90° and ±135°). During the simulation, dislocation emission on each slip system pair is considered separately. Therefore, different branches may contain different numbers of dislocations as the simulation progresses.

The resulting transition behaviors for different loading rates are plotted as applied stress intensity versus temperature in Figs. 5 and 6 for the four and six-slip system cases, respectively. Kinks in the curves occur when the same number of dislocations is emitted at fracture for more than one temperature. Then the dislocation arrays spread farther at the higher temperature and shield the tip less. With only minor variation, the curves for applied stress intensity are shifted only by the change in loading rate, with higher loading rates giving rise to higher BDT temperatures. The same shift occurs in the number of dislocations versus temperature curves (not shown).

It is noted that the dislocation arrays at transition are nearly the same for all loading rates. These are shown for the four-slip system case in Fig. 7. As seen more clearly in the close-up, only the $\dot{K}_I^\infty/K_{Ic}$ = 100/sec arrays are slightly different as a few more dislocations were emitted at transition. All the other simulations showed even better agreement. The similarity of the arrays indicates that the plastic zone size required for a transition to ductile behavior is independent of the loading rate, which agrees with observations made in [21].

For comparison, the transition behaviors at a single loading rate ($\dot{K}_I^\infty/K_{Ic}$ = 1/sec) for two, four and six slip systems are shown in Figs. 8 and 9. Figure 8 shows the applied stress intensity at fracture versus temperature, and Fig. 9 shows the total number of dislocations for all slip systems emitted at fracture versus temperature. It is seen that, as the number of active slip systems increases, the transition becomes sharper. The sharpest transition occurs with a sudden jump in the number of emitted dislocations.

The transition curves for four slip systems at ±70° and ±110° are included in Figs. 8 and 9 to illustrate that the behavior depends on the actual angles chosen. Planes closer to 70.53° have higher resolved shear stresses for dislocation nucleation, provide stronger shielding, and result in a sharper transition behavior.

5. Discussion

It is shown in Figs. 4 and 9 that sharper transitions involve relatively fewer dislocations than gradual transitions. Examination of the dislocation distributions reveals that the dislocations remain close to the crack tip when the transition is sharp, and therefore only a relatively small number of dislocations are needed to provide strong shielding to the crack tip. This turns out to be the most important effect of the inter-branch dislocation interactions on the simulations with two slip systems. With the two slip systems at either ±45° or ±90°, each with the same number of dislocations, the effect of inter-branch interaction is to spread the dislocation distribution to about twice the size as that without interaction forces. Conversely, the distribution for the ±135° system is about twice as spread out when the interaction forces are not included compared with that with interactions accounted for. With multiple slip systems, the effects of the interaction forces are compensated by being able to pack more dislocations close to the crack tip since the dislocations are on different planes.

To illustrate the importance of both near-tip dislocation density and shielding effectiveness of various planes, the dislocation arrays for two, four and six slip systems are illustrated in Fig. 10. These are all at the moment of brittle fracture with 50 total dislocations and different temperatures and applied loads. The 45°/135° system provides very similar shielding to the 90° system (see Fig. 8). The higher near-tip dislocation density of the 45°/135° system is necessary to compensate for the reduction in shielding effectiveness of these angles compared with 90°. The near-tip dislocation density becomes much more important for the six slip systems. For the same total number of dislocations, the plastic zone size at fracture for four slip systems is six times larger than the zone for six slip systems. Therefore, the shielding was nearly twice as strong for six slip systems.

As noted in the introduction, Qian and Li [25, 26] have modeled dislocation distributions at the crack tip at equilibrium for multiple slip systems. Such equilibrium models are not suited to modeling actual fracture experiments because the experiments occur on a time scale much faster than the time scale for equilibrium [6]. Discussion of their results is interesting because they observed different behavior concerning the order of dislocation nucleation and the effect of multiple slip systems on shielding. The differences may stem more from their algorithm than from an equilibrium versus dynamic modeling argument. Their algorithm involved introducing new dislocations near the crack tip and allowing any of the dislocations to move one Burgers vector at a time so long as its slip force is greater than the lattice friction. Dislocation motion continued after each nucleation event until equilibrium was reached. Two nucleation scenarios were investigated: sequential emission [25] where one pair of dislocations was nucleated on the symmetric planes with the highest slip force, and simultaneous emission [26] where a pair of dislocations was nucleated on every pair of planes with a slip force exceeding the lattice friction.

Even with a big difference in friction stress between their models and the present model, the resulting dislocation distributions for four slip systems (Fig. 10 here compared with Fig. 10 of [25] and Fig. 3 of [26]) are similar in terms of array size and total dislocations for a similar applied load and similar slip system angles. The difference is in the order of dislocation nucleation. In the present model, dislocations were emitted in a pattern of one at 45°, one at 135°, two at 45°, one at 135°, and then repeating to give a

3/2 ratio between the 45° and the 135° systems. This ratio may depend sensitively on the selection of slip plane angles at the crack tip. This alternating emission of dislocations in different planes is also observed in the simulation with six slip systems.

In sequential emission, they reported that the 60° slip planes saturated first and then emission switched to the 120° planes. This is a direct consequence of waiting for equilibrium between each nucleation event. As they have shown [25], nucleation is preferred on the 70° plane where the crack tip stress field is highest. Thus, by waiting between each nucleation, the sources nearest 70° are freed up to nucleate again, rather than being shut down by the back stress of the previous dislocation. If nucleation were allowed at any time when the stress at the source exceeds the friction stress, then other slip systems would be activated in an alternating pattern.

In their simultaneous emission simulations, dislocations are forced into each slip system until the 120° planes are saturated and then the 60° plane continues alone until saturation. The ratio ends up close to the 2/3 seen in our simulation, but forcing simultaneous emission seems physically unrealistic. Although it has been shown that there is no interaction force between sources along a circle about the crack tip [27], the source with the highest stress would be activated first and its dislocation would interact with the other sources as soon as it moves. Sources nearby in terms of slip system angle would probably be shut down, but the effect on other sources cannot be assumed. The decrease in shielding effectiveness for more slip systems with the same total number of dislocations is a direct consequence of forced emission.

Our results showed qualitatively what the influences of inter-branch interaction forces and multiple slip systems are on the BDT behavior. However, the actual transition temperatures predicted by our simulations are much too low. Compared with the summary of experimental results in [7], the BDT temperatures predicted by our simulations are about 400°C too low. The shielding provided by dislocations completely parallel to the crack front (as is the case for the present 2D simulation) is much larger than that by real 3D dislocations. Other structure-dependent modifications, such as atomic step formation at the crack tip due to dislocation nucleation or crack tip blunting, must be included to adjust the transition temperature. Although these results are only qualitative, they do show the influence of multiple slip systems and can help us understand why the transition in silicon can be so sharp.

6. Conclusions

The present study shows that, although the interaction forces between dislocations in different slip systems are small, their influence on the brittle-ductile transition behavior is significant. They should be included in any such dynamic dislocation simulation.

Multiple slip systems increase the crack tip shielding by increasing the near tip dislocation density. Thus, fewer dislocations can be more effective at shielding the crack tip. The brittle-ductile transition occurs sharply when the dislocation number can increase rapidly while the dislocation array is still compact around the crack tip.

The sharpness of the brittle-ductile transition in silicon is strongly dependent on the number of active slip systems. The predicted transition behavior by the present simulations sharpens as the number of slip systems approaches the experimentally determined number. This dependence may be checked in tests that suppress certain slip systems.

Acknowledgments

This work is supported by the National Science Foundation through grant No. CMS 95-22661. BDF is supported by a NSF Graduate Fellowship. Helpful discussion with Dr. R. Thomson of NIST is gratefully acknowledged.

References

1. W.J. Broad, New Idea on Titanic Sinking Faults Steel as Main Culprit, New York Times, Sept. 16, 1993.
2. C. St. John, Phil. Mag. 32 (1975) 1193.
3. M. Brede, P. Haasen, Acta Metall. 36 (1988) 2003.
4. J. Samuels, S.G. Roberts, Proc. R. Soc. Lond. A 421 (1989) 1.
5. P.B. Hirsch, F.R.S., S.G. Roberts, J. Samuels, Proc. R. Soc. Lond. A 421 (1989) 25.
6. S.G. Roberts, M. Ellis, P.B. Hirsch, Mater. Sci. Eng. A 164 (1993) 135.
7. S.G. Roberts, A.S. Booth, P.B. Hirsch, Mater. Sci. Eng. A 176 (1994) 91.
8. P.B. Hirsch, S.G. Roberts, Acta Mater. 44 (1996) 2361.
9. M. Brede, Acta Metall. Mater. 41 (1993) 211.
10. Y.-B. Xin, K.J. Hsia, Acta Mater. 45 (1997) 1747.
11. P.B. Hirsch, S.G. Roberts, Scripta Mater. 37 (1997) 1901.
12. K.J. Hsia, Y.-B. Xin, Scripta Mater. 37 (1997) 1905.
13. J.R. Rice, R. Thomson, Phil. Mag. 29 (1974) 73.
14. J.R. Rice, J. Mech. Phys. Solids 40 (1992) 239.
15. J.R. Rice, G.E. Beltz, Y. Sun, Peierls framework for dislocation nucleation from a crack tip, in: A.S. Argon (Ed.), Topics in Fracture and Fatigue, Springer-Verlag, New York, 1992, pp. 1-58.
16. G. Xu, A.S. Argon, M. Ortiz, Phil. Mag. A 72 (1995) 415.
17. M. Khantha, D.P. Pope, V.Vitek, Scripta Metall. Mater. 31 (1994) 1349.
18. Y.-B. Xin, K.J. Hsia, Acta Mater. 44 (1996) 845.
19. K.J. Hsia, Y.-B. Xin, T.J. Lagger, and M.J. Busche, unpublished research at the University of Illinois, Urbana, IL, 1995-1999.
20. G. Michot, On the Sharpness of the Brittle-to-Ductile Transition, presented at the Simulation of Microstructure and Strength of Materials Workshop, Stuttgart, Germany, July 20-21, 1998.
21. A. George, G. Michot, Mater. Sci. Eng. A 164 (1993) 118.
22. P.D. Warren, Scripta Metall. 23 (1989) 637.
23. G. Michot, M.A. Loyola de Oliveira, H. Koizumi, J. Phys. IV France 8 (1998) 145.
24. V. Lakshmanan, J.C.M. Li, Mater. Sci. Eng. A 104 (1988) 95.
25. C.-F. Qian, J.C.M. Li, Mech. Mater. 24 (1996) 1.
26. C.-F. Qian, J.C.M. Li, Mech. Mater. 24 (1996) 11.
27. C.-F. Qian, K. Li, H. Chen, J.C.M. Li, Mech. Mater. 24 (1996) 221.
28. I.-H. Lin, R. Thomson, Acta Metall. 34 (1986) 187.
29. M. Imai, K. Sumino, Phil. Mag. A 47 (1983) 599.

Appendix

Lakshmanan and Li [24] substituted the image distribution of Burgers vectors caused by a single dislocation in the presence of a crack into the equations for the stress field of a single edge dislocation. By integrating the result over the crack plane and adding the stress field of the dislocation itself, they arrived at an expression for the forces on a dislocation with Burgers vector $b_i \exp(i\phi_i)$ at any position in the complex plane, $z_i=r_i \exp(i\theta_i)$, due to a dislocation with Burgers vector $b_j \exp(i\phi_j)$ at $z_j=r_j \exp(i\theta_j)$. The crack lies along the negative real axis. The real and imaginary parts are Re(.) and Im(.), respectively. Also μ is the shear modulus, ν is the Poisson's ratio, and K_I^{∞} is the far-field stress intensity. The image, interaction and crack tip stresses can be written as

$$\tau_{kd} = \frac{K_I^{\infty}}{\sqrt{2\pi|z_i|}} \sin\left(\frac{\theta_i}{2}\right) \cos^2\left(\frac{\theta_i}{2}\right)$$

$$\tau_{d^2} = \frac{\mu}{2\pi(1-\nu)} [\cos(2\phi_i)\mathrm{Re}(B_x + B) - \sin(2\phi_i)\mathrm{Im}(B_x + B)] \tag{A1}$$

$$\tau_{dd_j} = \frac{\mu}{2\pi(1-\nu)} [\cos(2\phi_i)\mathrm{Re}(B_x + B_{0x} + B + B_0) - \sin(2\phi_i)\mathrm{Im}(B_x + B_{0x} + B + B_0)]$$

where B_x, B_{0x}, B and B_0 are given as

$$B_x = b_j (A_1 X_1 + A_2 X_2 + A_3 X_3 + A_4 X_4)$$

$$B_{0x} = \frac{b_j \cos\phi_j}{z_i - z_j} \tag{A2}$$

$$B = ib_j \,\mathrm{Im}(z_i)(A_5 Z_1 + A_6 Z_2 + A_7 Z_3)$$

$$B_0 = -\frac{ib_j}{(z_i - z_j)^2} [\mathrm{Im}(z_i) - \mathrm{Im}(z_j)][\cos(\phi_j) + i\sin(\phi_j)]$$

where A_n (n=1, 2, …, 7) are

$$A_1 = \frac{-1}{z_i^{1/2}\left(z_i^{1/2} + \bar{z}_j^{1/2}\right)}$$

$$A_2 = \frac{-1}{z_i^{1/2}\left(z_i^{1/2} + z_j^{1/2}\right)}$$

$$A_3 = -\frac{2\bar{z}_j^{1/2} z_j + z_i^{1/2} z_j + z_i^{1/2}\bar{z}_j}{2z_i^{1/2}\bar{z}_j\left(z_i^{1/2} + \bar{z}_j^{1/2}\right)^2}$$

$$A_4 = -\frac{2z_j^{1/2}\bar{z}_j + z_i^{1/2}\bar{z}_j + z_i^{1/2}z_j}{2z_i^{1/2}z_j\left(z_i^{1/2}+z_j^{1/2}\right)^2} \tag{A3}$$

$$A_5 = \frac{\bar{z}_j^{1/2} + 2z_i^{1/2}}{2z_i^{3/2}\left(z_i^{1/2}+\bar{z}_j^{1/2}\right)^2}$$

$$A_6 = \frac{z_j^{1/2} + 2z_i^{1/2}}{2z_i^{3/2}\left(z_i^{1/2}+z_j^{1/2}\right)^2}$$

$$A_7 = \frac{z_j\bar{z}_j + z_i\bar{z}_j + 3z_i^{1/2}z_j\bar{z}_j^{1/2} + z_iz_j}{2z_i^{3/2}\bar{z}_j\left(z_i^{1/2}+\bar{z}_j^{1/2}\right)^3}$$

and X_n (n=1, 2, 3, 4), Y_n (n=1, 2, 3) and Z_n (n=1, 2, 3) are

$$X_1 = \frac{1}{4}\exp\left(i\phi_j\right) + \frac{1}{8}\exp\left\{i\left(-\phi_j\right)\right\} - \frac{1}{8}\exp\left\{i\left(-\phi_j + 2\theta_j\right)\right\}$$

$$X_2 = \overline{X}_1$$

$$X_3 = \frac{1}{4}\exp\left\{i\left(-\phi_j\right)\right\}$$

$$X_4 = \overline{X}_3 \tag{A4}$$

$$Y_1 = -\frac{i}{4}\exp\left(i\phi_j\right) + \frac{3i}{8}\exp\left\{i\left(-\phi_j\right)\right\} + \frac{i}{8}\exp\left\{i\left(-\phi_j + 2\theta_j\right)\right\}$$

$$Y_2 = \overline{Y}_1$$

$$Y_3 = -\frac{i}{4}\exp\left\{i\left(-\phi_j\right)\right\}$$

$$Z_1 = X_1 + iY_1$$

$$Z_2 = X_2 + iY_2$$

$$Z_3 = X_3 + iY_3$$

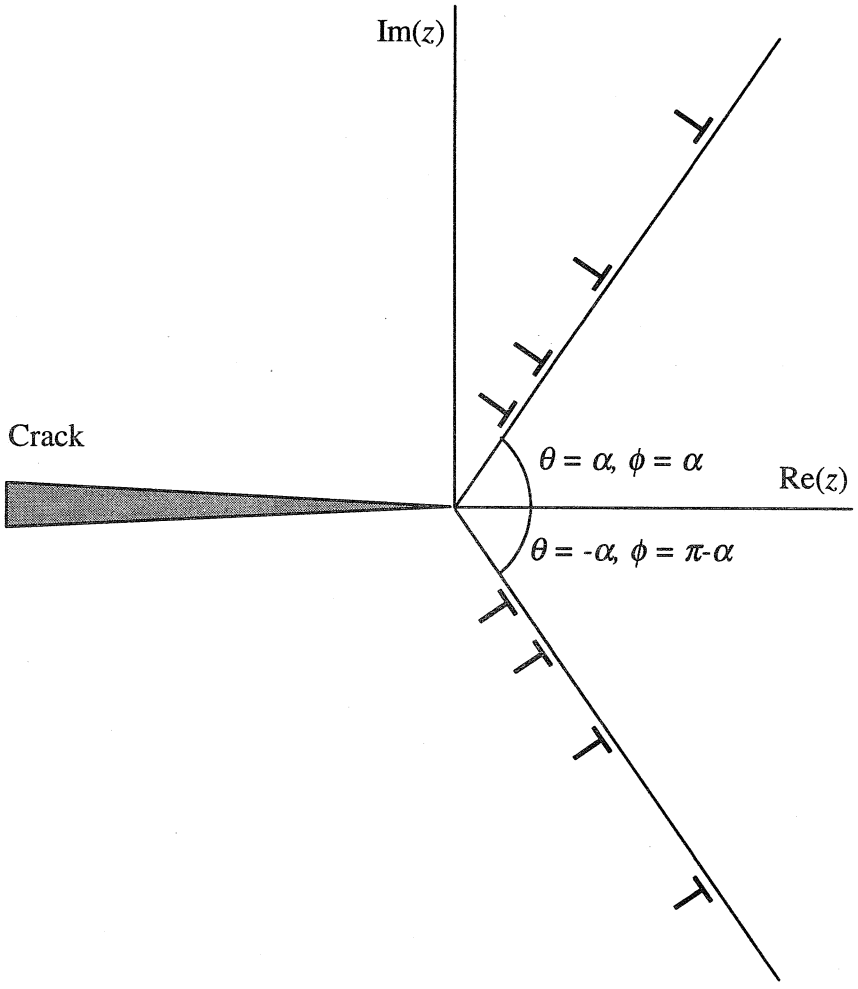

Figure 1 Model with a pair of symmetric slip systems at a general angle α. Slip planes lie in the θ direction and Burgers vectors point in the ϕ direction.

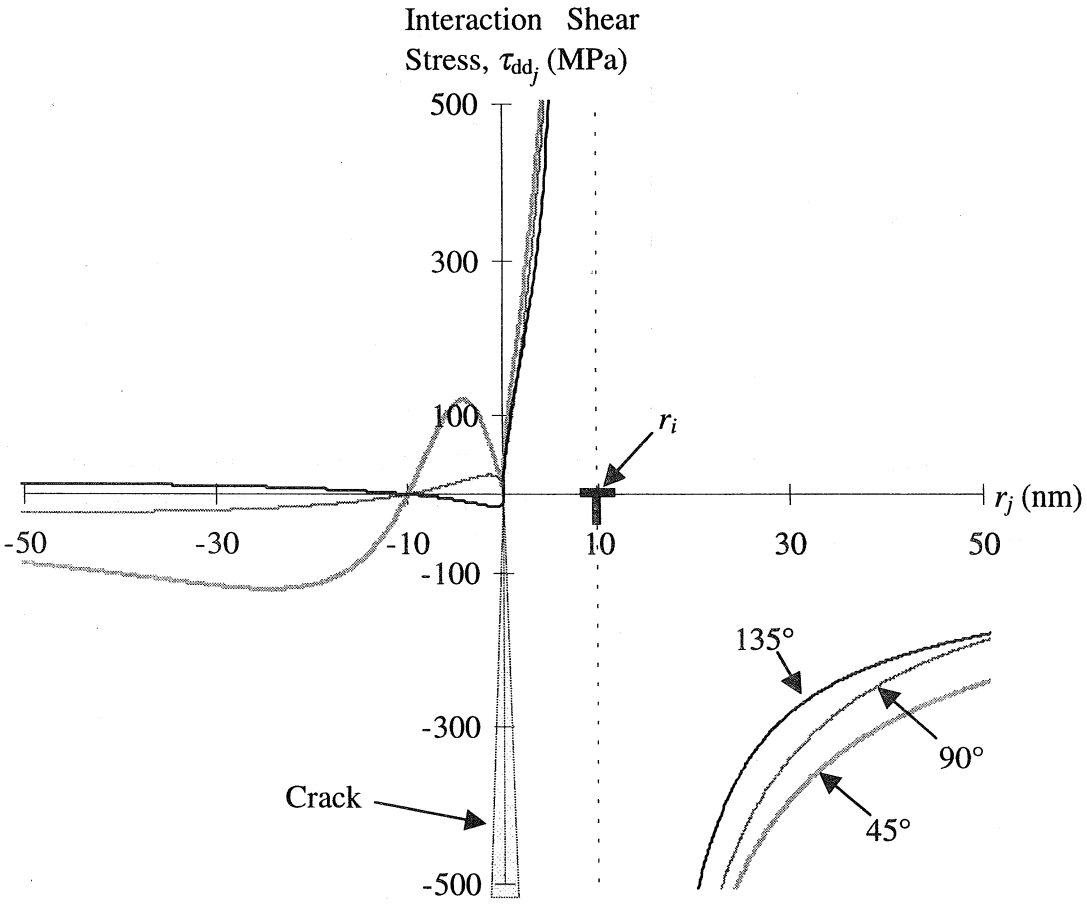

Figure 2 Interaction shear stress on a dislocation at r_i (fixed) due to a dislocation at r_j (variable).

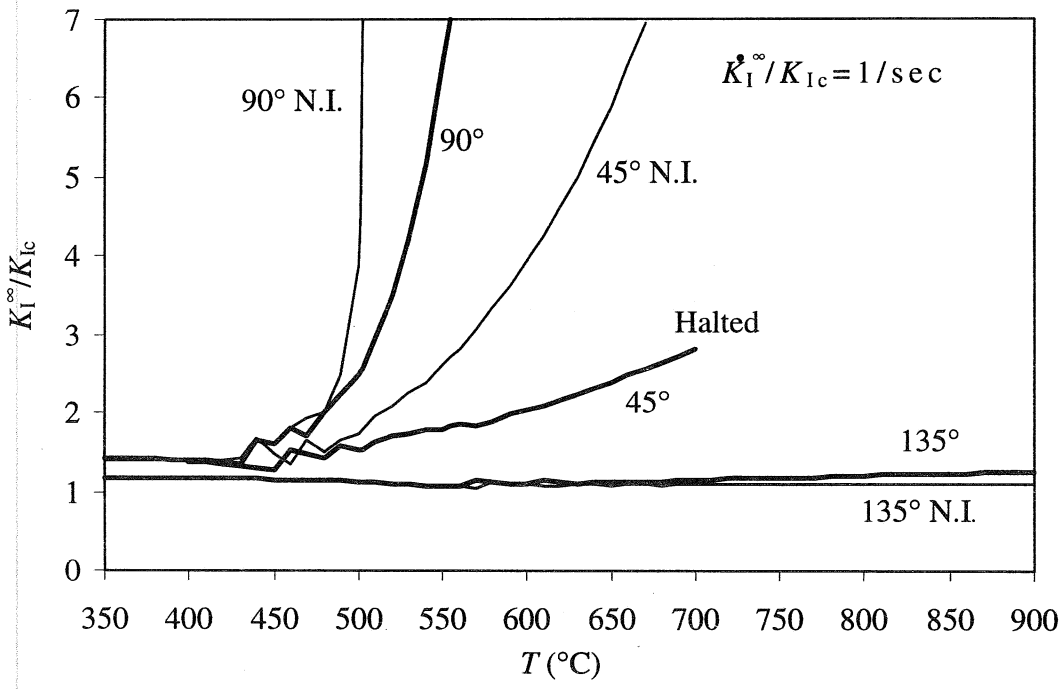

Figure 3 Applied stress intensity at fracture for different angles with or without inter-branch interaction forces. The simulation was performed only up to 700°C for the ±45° systems. N.I. represents no interaction.

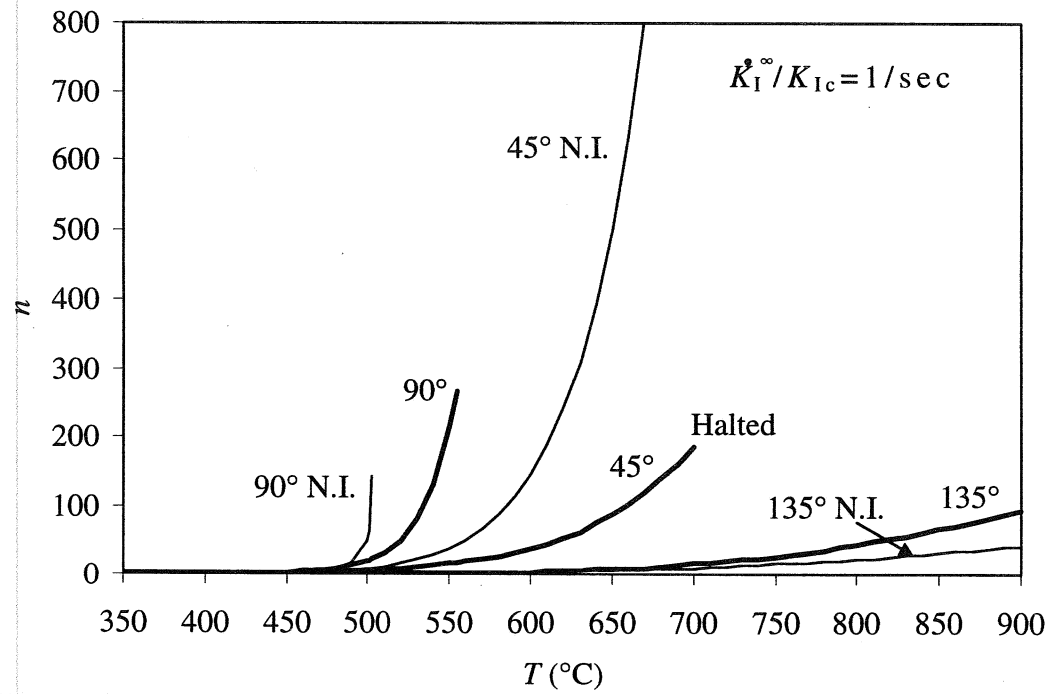

Figure 4 Total dislocations produced at fracture for different angles with or without inter-branch interaction forces. The simulation was performed only up to 700°C for the ±45° systems. N.I. represents no interaction.

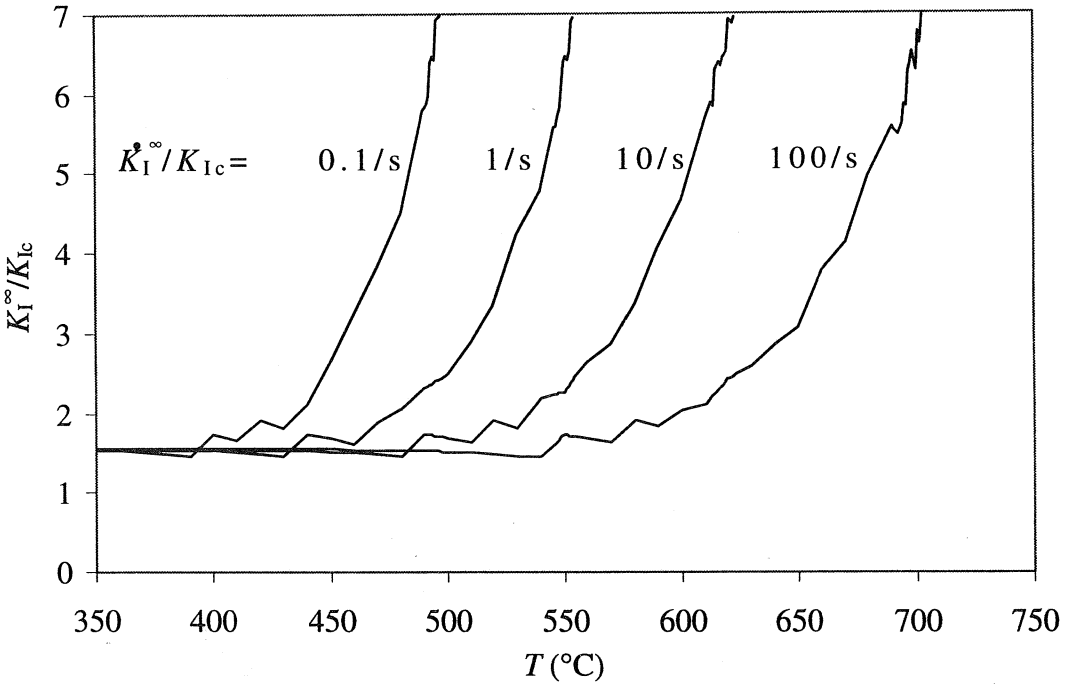

Figure 5 Applied stress intensity at fracture for four slip systems (±45°, ±135°) at different loading rates.

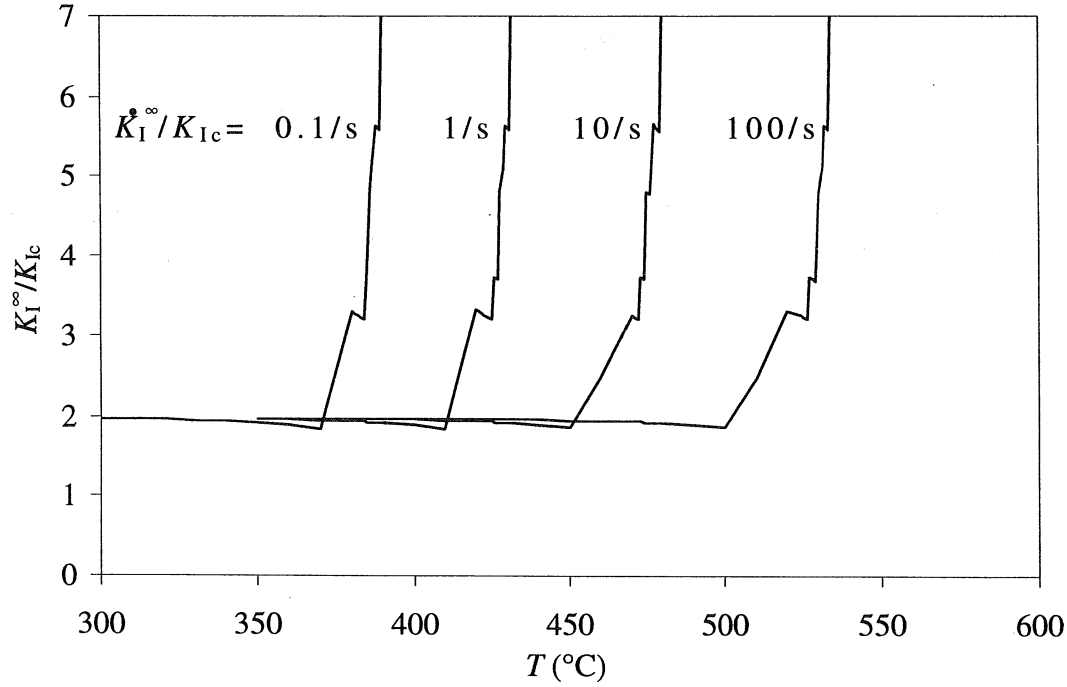

Figure 6 Applied stress intensity at fracture for six slip systems (±45°, ±90°, ±135°) at different loading rates.

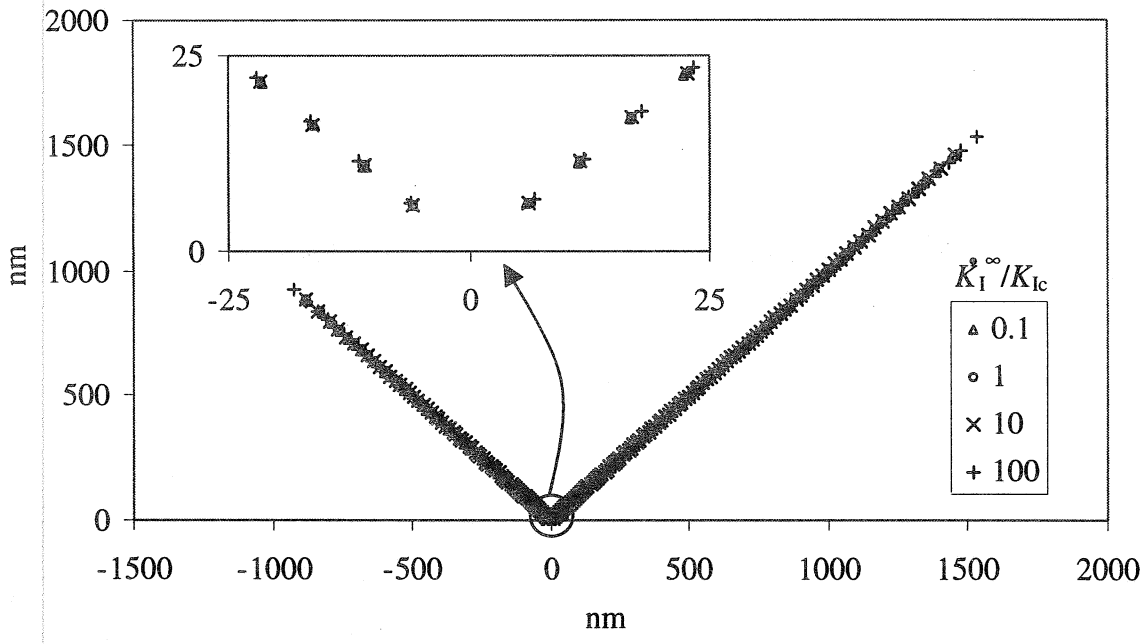

Figure 7 Dislocation arrays at different loading rates at the moment of fracture at the BDT temperature.

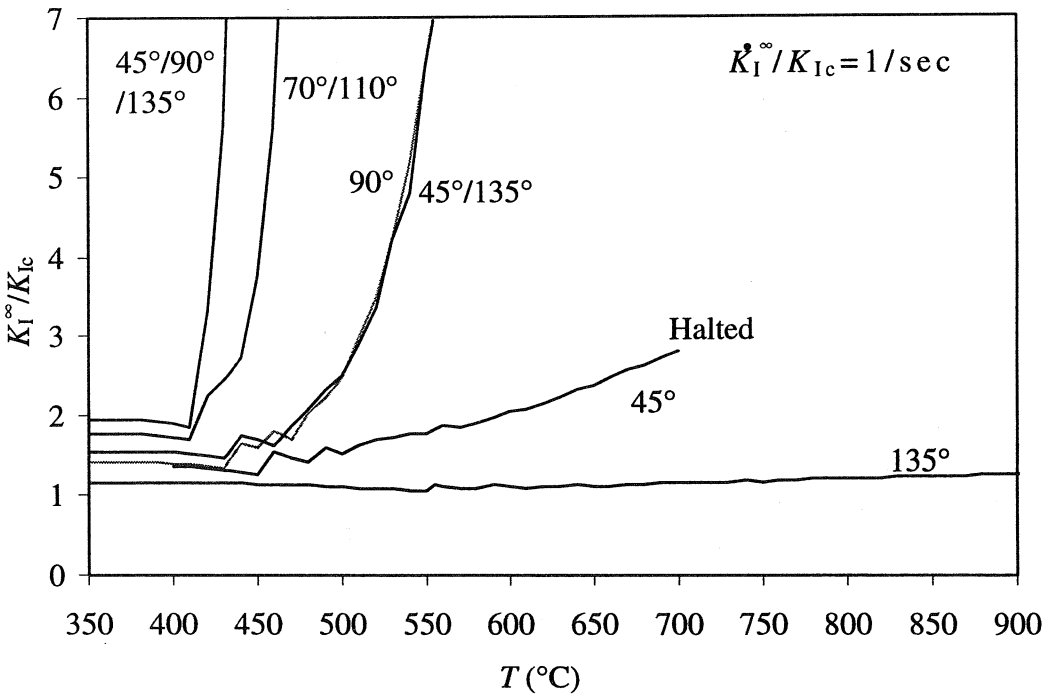

Figure 8 Effect of multiple slip systems on applied stress intensity at fracture.

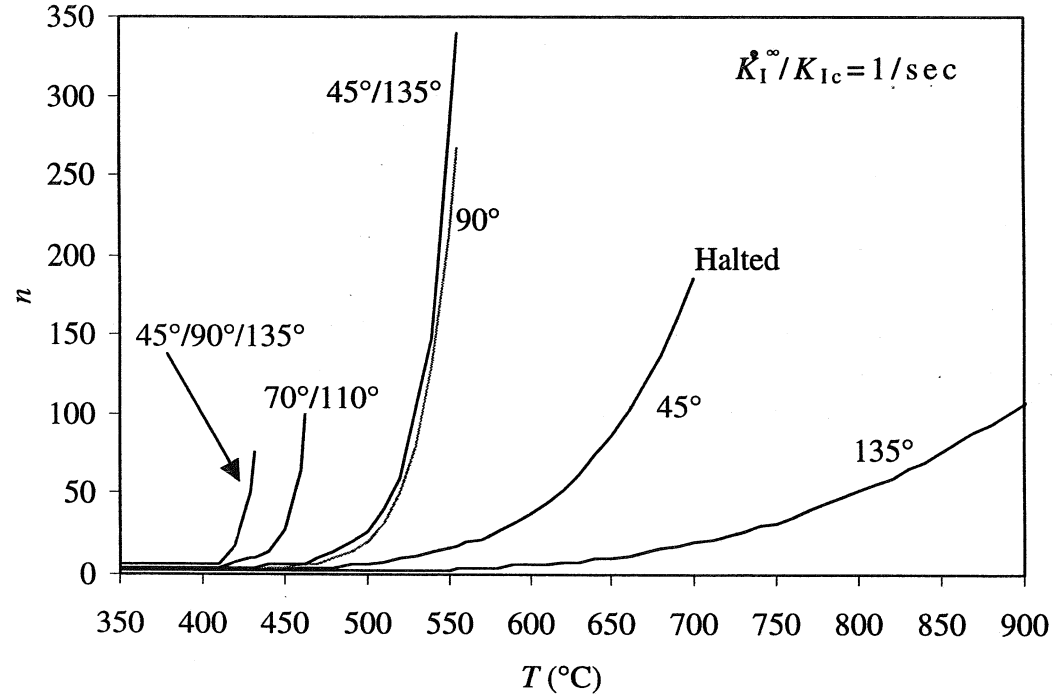

Figure 9 Effect of multiple slip systems on total dislocations emitted at fracture.

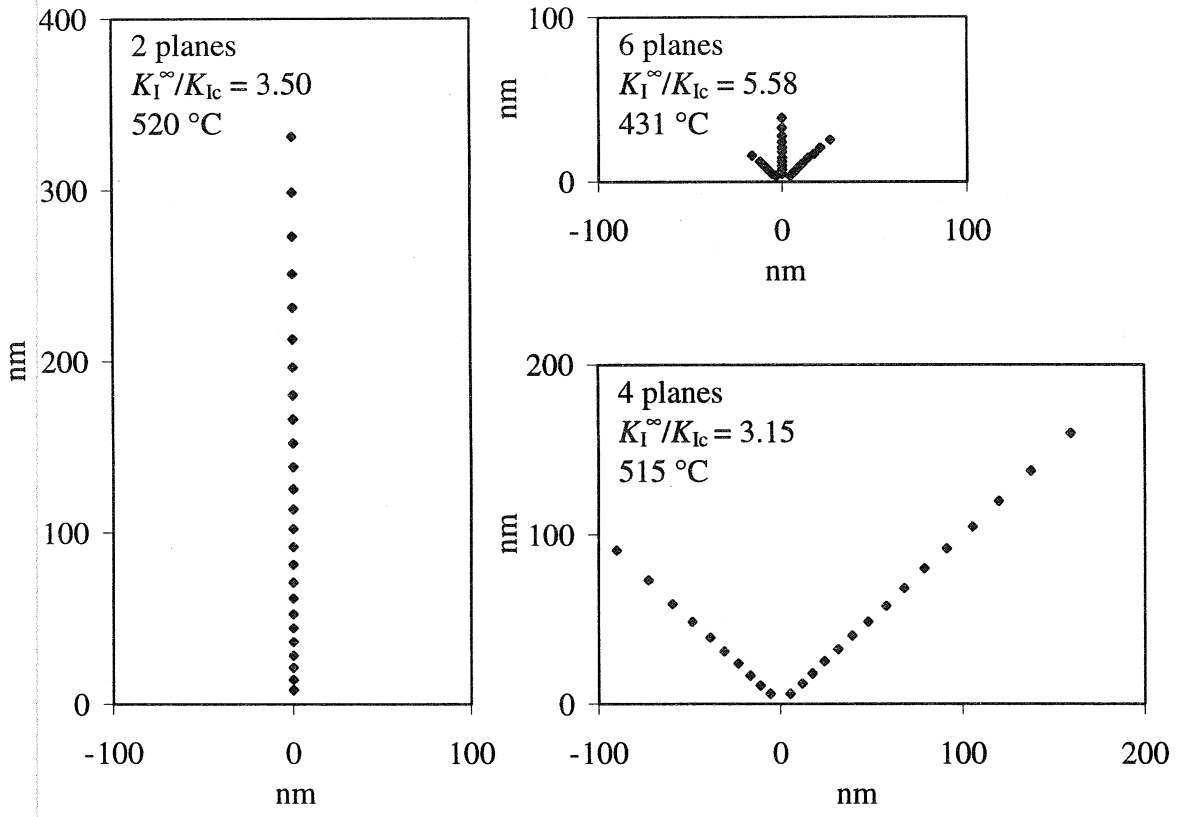

Figure 10 Dislocation arrays in the upper half plane for two, four and six slip systems. All three cases are for a loading rate of $\dot{K}_I^\infty/K_{Ic}$ =1/sec and are shown at the moment of brittle failure with 50 total dislocations.

List of Recent TAM Reports

No.	Authors	Title	Date
809	Xin, Y.-B., and K. J. Hsia	Simulation of the brittle–ductile transition in silicon single crystals using dislocation mechanics—*Acta Metallurgica et Materialia* **45**, 1747–1759 (1997)	Oct. 1995
810	Ulysse, P., and R. E. Johnson	A plane-strain upper-bound analysis of unsymmetrical single-hole and multi-hole extrusion processes	Oct. 1995
811	Fried, E.	Continua described by a microstructural field—*Zeitschrift für angewandte Mathematik und Physik* **47**, 168–175 (1996)	Nov. 1995
812	Mittal, R., and S. Balachandar	Autogeneration of three-dimensional vortical structures in the near wake of a circular cylinder	Nov. 1995
813	Segev, R., E. Fried, and G. de Botton	Force theory for multiphase bodies—*Journal of Geometry and Physics* **20**, 371–392 (1996)	Dec. 1995
814	Weaver, R. L.	The effect of an undamped finite-degree-of-freedom "fuzzy" substructure: Numerical solutions and theoretical discussion—*Journal of the Acoustical Society of America* **100**, 3159–3164 (1996)	Jan. 1996
815	Haber, R. B., C. S. Jog, and M. P. Bendsøe	A new approach to variable-topology shape design using a constraint on perimeter—*Structural Optimization* **11**, 1–12 (1996)	Feb. 1996
816	Xu, Z.-Q., and K. J. Hsia	A numerical solution of a surface crack under cyclic hydraulic pressure loading—*ASME Journal of Tribology* **119**, 637–645 (1997)	Mar. 1996
817	Adrian, R. J.	Bibliography of particle velocimetry using imaging methods: 1917–1995—*Produced and distributed in cooperation with TSI, Inc., St. Paul, Minn.*	Mar. 1996
818	Fried, E., and G. Grach	An order-parameter based theory as a regularization of a sharp-interface theory for solid–solid phase transitions—*Archive for Rational Mechanics and Analysis* **138**, 355–404 (1997)	Mar. 1996
819	Vonderwell, M. P., and D. N. Riahi	Resonant instability mode triads in the compressible boundary-layer flow over a swept wing—*International Journal of Engineering Science* **36**, 599–624 (1998)	Mar. 1996
820	Short, M., and D. S. Stewart	Low-frequency two-dimensional linear instability of plane detonation—*Journal of Fluid Mechanics* **340**, 249–295 (1997)	Mar. 1996
821	Casagranda, A., and P. Sofronis	On the scaling laws for the consolidation of nanocrystalline powder compacts—Proceedings of the *IUTAM Symposium on the Mechanics of Granular and Porous Materials*, N. A. Fleck and A. C. F. Cocks, eds. The Netherlands: Kluwer Academic Publishers, 105–116 (1997)	Apr. 1996
822	Xu, S., and D. S. Stewart	Deflagration-to-detonation transition in porous energetic materials: A comparative model study—*Journal of Engineering Mathematics* **31**, 143–172 (1997)	Apr. 1996
823	Weaver, R. L.	Mean and mean-square responses of a prototypical master/fuzzy structure—*Journal of the Acoustical Society of America* **101**, 1441–1449 (1997)	Apr. 1996
824	Fried, E.	Correspondence between a phase-field theory and a sharp-interface theory for crystal growth—*Continuum Mechanics and Thermodynamics* **9**, 33–60 (1997)	Apr. 1996
825	Students in TAM 293–294	Thirty-third student symposium on engineering mechanics, J. W. Phillips, coordinator: Selected senior projects by W. J. Fortino II, A. A. Mordock, and M. R. Sawicki	May 1996
826	Riahi, D. N.	Effects of roughness on nonlinear stationary vortices in rotating disk flows—*Mathematical and Computer Modeling* **25**, 71–82 (1997)	June 1996
827	Riahi, D. N.	Nonlinear instabilities of shear flows over rough walls, *Far East Journal of Applied Mathematics*, in press (1998)	June 1996
828	Weaver, R. L.	Multiple scattering theory for a plate with sprung masses, mean responses—*Journal of the Acoustical Society of America* **101**, 3466–3414 (1997)	July 1996
829	Moser, R. D., M. M. Rogers, and D. W. Ewing	Self-similarity of time-evolving plane wakes *Journal of Fluid Mechanics*, in press (1998)	July 1996

List of Recent TAM Reports (cont'd)

No.	Authors	Title	Date
830	Lufrano, J. M., and P. Sofronis	Enhanced hydrogen concentrations ahead of rounded notches and cracks: Competition between plastic strain and hydrostatic stress—*Acta Metallurgica et Materialia,* in press (1998)	July 1996
831	Riahi, D. N.	Effects of surface corrugation on primary instability modes in wall-bounded shear flows	Aug. 1996
832	Bechel, V. T., and N. R. Sottos	Application of debond length measurements to examine the mechanics of fiber pushout	Aug. 1996
833	Riahi, D. N.	Effect of centrifugal and Coriolis forces on chimney convection during alloy solidification—*Journal of Crystal Growth* **179** , 287–296 (1997)	Sept. 1996
834	Cermelli, P., and E. Fried	The influence of inertia on configurational forces in a deformable solid—*Proceedings of the Royal Society of London A* **453**, 1915–1927 (1997)	Oct. 1996
835	Riahi, D. N.	On the stability of shear flows with combined temporal and spatial imperfections	Oct. 1996
836	Carranza, F. L., B. Fang, and R. B. Haber	An adaptive space–time finite element model for oxidation-driven fracture, *Computer Methods in Applied Mechanics and Engineering*, in press (1997)	Nov. 1996
837	Carranza, F. L., B. Fang, and R. B. Haber	A moving cohesive interface model for fracture in creeping materials, *Computational Mechanics* **19**, 517–521 (1997)	Nov. 1996
838	Balachandar, S., R. Mittal, and F. M. Najjar	Properties of the mean wake recirculation region in two-dimensional bluff body wakes—*Journal of Fluid Mechanics*, in press (1997)	Dec. 1996
839	Ti, B. W., W. D. O'Brien, Jr., and J. G. Harris	Measurements of coupled Rayleigh wave propagation in an elastic plate—*Journal of the Acoustical Society of America* **102**, 1528–1531	Dec. 1996
840	Phillips, W. R. C.	On finite-amplitude rotational waves in viscous shear flows—*Studies in Applied Mathematics* **100**, in press (1998)	Jan. 1997
841	Riahi, D. N.	Direct resonance analysis and modeling for a turbulent boundary layer over a corrugated surface—*Acta Mechanica*, in press (1998)	Jan. 1997
842	Liu, Z.-C., R. J. Adrian, C. D. Meinhart, and W. Lai	Structure of a turbulent boundary layer using a stereoscopic, large format video-PIV—*Developments in Laser Techniques and Fluid Mechanics*, 259–273 (1997)	Jan. 1997
843	Fang, B., F. L. Carranza, and R. B. Haber	An adaptive discontinuous Galerkin method for viscoplastic analysis—*Computer Methods in Applied Mechanics and Engineering* **150**, 191–198 (1997)	Jan. 1997
844	Xu, S., T. D. Aslam, and D. S. Stewart	High-resolution numerical simulation of ideal and non-ideal compressible reacting flows with embedded internal boundaries—*Combustion Theory and Modeling* **1**, 113–142 (1997)	Jan. 1997
845	Zhou, J., C. D. Meinhart, S. Balachandar, and R. J. Adrian	Formation of coherent hairpin packets in wall turbulence—In *Self-Sustaining Mechanisms in Wall Turbulence*, R. L. Panton, ed. Southampton, UK: Computational Mechanics Publications, 109–134 (1997)	Feb. 1997
846	Lufrano, J. M., P. Sofronis, and H. K. Birnbaum	Elastoplastically accommodated hydride formation and embrittlement—*Journal of Mechanics and Physics of Solids*, in press (1998)	Feb. 1997
847	Keane, R. D., N. Fujisawa, and R. J. Adrian	Unsteady non-penetrative thermal convection from non-uniform surfaces—In *Geophysical and Astrophysical Convection*, R. Kerr, ed. (1997)	Feb. 1997
848	Aref, H., and M. Brøns	On stagnation points and streamline topology in vortex flows—*Journal of Fluid Mechanics* **370**, 1–27 (1998)	Mar. 1997
849	Asghar, S., T. Hayat, and J. G. Harris	Diffraction by a slit in an infinite porous barrier—*Wave Motion*, in press (1998)	Mar. 1997
850	Shawki, T. G., H. Aref, and J. W. Phillips	Mechanics on the Web—Proceedings of the International Conference on Engineering Education (Aug. 1997, Chicago)	Apr. 1997

No.	Authors	Title	Date
851	Stewart, D. S., and J. Yao	The normal detonation shock velocity–curvature relationship for materials with non-ideal equation of state and multiple turning points—*Combustion and Flame*, in press (1998)	Apr. 1997
852	Fried, E., A. Q. Shen, and S. T. Thoroddsen	Wave patterns in a thin layer of sand within a rotating horizontal cylinder—*Physics of Fluids* **10**, 10–12 (1998)	Apr. 1997
853	Boyland, P. L., H. Aref, and M. A. Stremler	Topological fluid mechanics of stirring	Apr. 1997
854	Parker, S. J., and S. Balachandar	Viscous and inviscid instabilities of flow along a streamwise corner—*Theoretical and Computational Fluid Dynamics*, in press (1997)	May 1997
855	Soloff, S. M., R. J. Adrian, and Z.-C. Liu	Distortion compensation for generalized stereoscopic particle image velocimetry—*Measurement Science and Technology* **8**, 1–14 (1997)	May 1997
856	Zhou, Z., R. J. Adrian, S. Balachandar, and T. M. Kendall	Mechanisms for generating coherent packets of hairpin vortices in near-wall turbulence—*Journal of Fluid Mechanics*, in press (1997)	June 1997
857	Neishtadt, A. I., D. L. Vainshtein, and A. A. Vasiliev	Chaotic advection in a cubic stokes flow—*Physica D* **111**, 227 (1997).	June 1997
858	Weaver, R. L.	Ultrasonics in an aluminum foam—*Ultrasonics*, in press (1997)	July 1997
859	Riahi, D. N.	High gravity convection in a mushy layer during alloy solidification—In *Nonlinear Instability, Chaos and Turbulence*, D. N. Riahi and L. Debnath, eds., in press (1998)	July 1997
860	Najjar, F. M., and S. Balachandar	Low-frequency unsteadiness in the wake of a normal plate, *Journal of Fluid Mechanics*, in press (1997)	Aug. 1997
861	Short, M.	A parabolic linear evolution equation for cellular detonation instability	Aug. 1997
862	Short, M., and D. S. Stewart	Cellular detonation stability—I: A normal-mode linear analysis	Sept. 1997
863	Carranza, F. L., and R. B. Haber	A numerical study of intergranular fracture and oxygen embrittlement in an elastic–viscoplastic solid—*Journal of the Mechanics and Physics of Solids*, in press (1997)	Oct. 1997
864	Sakakibara, J., and R. J. Adrian	Whole-field measurement of temperature in water using two-color laser-induced fluorescence	Oct. 1997
865	Riahi, D. N.	Effect of surface corrugation on convection in a three-dimensional finite box of fluid-saturated porous material	Oct. 1997
866	Baker, C. F., and D. N. Riahi	Three-dimensional flow instabilities during alloy solidification	Oct. 1997
867	Fried, E.	Introduction (only) to *The Physical and Mathematical Foundations of the Continuum Theory of Evolving Phase Interfaces* (book containing 14 seminal papers dedicated to Morton E. Gurtin), Berlin: Springer-Verlag, in press (1998)	Oct. 1997
868	Folguera, A., and J. G. Harris	Coupled Rayleigh surface waves in a slowly varying elastic waveguide	Oct. 1997
869	Stewart, D. S.	Detonation shock dynamics: Application for precision cutting of metal with detonation waves	Oct. 1997
870	Shrotriya, P., and N. R. Sottos	Creep and relaxation behavior of woven glass/epoxy substrates for multilayer circuit board applications	Nov. 1997
871	Riahi, D. N.	Boundary wave–vortex interaction in channel flow at high Reynolds numbers, *Fluid Dynamics Research*, in press (1998)	Nov. 1997
872	George, W. K., L. Castillo, and M. Wosnik	A theory for turbulent pipe and channel flows—paper presented at *Disquisitiones Mechanicae* (Urbana, Ill., October 1996)	Nov. 1997
873	Aslam, T. D., and D. S. Stewart	Detonation shock dynamics and comparisons with direct numerical simulation	Dec. 1997

List of Recent TAM Reports (cont'd)

No.	*Authors*	*Title*	*Date*
874	Short, M., and A. K. Kapila	Blow-up in semilinear parabolic equations with weak diffusion	Dec. 1997
875	Riahi, D. N.	Analysis and modeling for a turbulent convective plume—*Mathematical and Computer Modeling* **28**, 57–63 (1998)	Jan. 1998
876	Stremler, M. A., and H. Aref	Motion of three point vortices in a periodic parallelogram	Feb. 1998
877	Dey, N., K. J. Hsia, and D. F. Socie	On the stress dependence of high-temperature static fatigue life of ceramics	Feb. 1998
878	Brown, E. N., and N. R. Sottos	Thermoelastic properties of plain weave composites for multilayer circuit board applications	Feb. 1998
879	Riahi, D. N.	On the effect of a corrugated boundary on convective motion	Feb. 1998
880	Riahi, D. N.	On a turbulent boundary layer flow over a moving wavy wall	Mar. 1998
881	Riahi, D. N.	Vortex formation and stability analysis for shear flows over combined spatially and temporally structured walls	June 1998
882	Short, M., and D. S. Stewart	The multi-dimensional stability of weak heat release detonations	June 1998
883	Fried, E., and M. E. Gurtin	Coherent solid-state phase transitions with atomic diffusion: A thermomechanical treatment—*Journal of Statistical Physics* (1998)	June 1998
884	Langford, J. A., and R. D. Moser	Optimal large-eddy simulation formulations for isotropic turbulence	July 1998
885	Riahi, D. N.	Boundary-layer theory of magnetohydrodynamic turbulent convection—*Proceedings of the Indian National Academy (Physical Science)*, in press (1998)	Aug. 1998
886	Riahi, D. N.	Nonlinear thermal instability in spherical shells—in *Nonlinear Instability, Chaos and Turbulence* **2**, in press (1998)	Aug. 1998
887	Riahi, D. N.	Effects of rotation on fully non-axisymmetric chimney convection during alloy solidification	Sept. 1998
888	Fried, E., and S. Sellers	The Debye theory of rotary diffusion	Sept. 1998
889	Short, M., A. K. Kapila, and J. J. Quirk	The hydrodynamic mechanisms of pulsating detonation wave instability	Sept. 1998
890	Stewart, D. S.	The shock dynamics of multidimensional condensed and gas phase detonations	Sept. 1998
891	Kim, K. C., and R. J. Adrian	Very large-scale motion in the outer layer	Oct. 1998
892	Fujisawa, N., and R. J. Adrian	Three-dimensional temperature measurement in turbulent thermal convection by extended range scanning liquid crystal thermometry	Oct. 1998
893	Shen, A. Q., E. Fried, and S. T. Thoroddsen	Is segregation-by-particle-type a generic mechanism underlying finger formation at fronts of flowing granular media?	Oct. 1998
894	Shen, A. Q.	Mathematical and analog modeling of lava dome growth	Oct. 1998
895	Buckmaster, J. D., and M. Short	Cellular instabilities, sub-limit structures, and edge-flames in premixed counterflows	Oct. 1998
896	Harris, J. G.	*Elastic waves*—Part of a book to be published by Cambridge University Press	Dec. 1998
897	Paris, A. J., and G. A. Costello	Cord composite cylindrical shells	Dec. 1998
898	Students in TAM 293–294	Thirty-fourth student symposium on engineering mechanics (May 1997), J. W. Phillips, coordinator: Selected senior projects by M. R. Bracki, A. K. Davis, J. A. (Myers) Hommema, and P. D. Pattillo	Dec. 1998
899	Taha, A., and P. Sofronis	A micromechanics approach to the study of hydrogen transport and embrittlement	Jan. 1999
900	Ferney, B. D., and K. J. Hsia	The influence of multiple slip systems on the brittle–ductile transition in silicon	Feb. 1999